2017

Identifying the Effects of a Human Dynein Mutation on GFP-Rab7 Axonal Transport in Embryonic Mouse Neurons

Natalie E. Wilson
University of Central Florida

IDENTIFYING THE EFFECTS OF A HUMAN DYNEIN MUTATION ON GFP-RAB7 AXONAL TRANSPORT IN EMBRYONIC MOUSE NEURONS

by

NATALIE E. WILSON

A thesis submitted in partial fulfillment of the requirements
for the Honors in the Major Program in Biomedical Sciences
in the Burnett School of Biomedical Sciences and the Burnett Honors College
at the University of Central Florida
Orlando, Florida

Spring Term, 2017

Thesis Chair: Dr. Stephen King

Abstract

The first dynein mutation found in humans that caused disease was a cytoplasmic dynein 1 heavy chain (*DYNC1H1* in humans) p.His306Arg mutation, first described by Weedon *et al.* in 2011. This mutation caused Charcot-Marie-Tooth (CMT) subtype 2O. CMT has a prevalence of approximately 1 in 2500 people, making it the most common hereditary neuromuscular disorder. Cytoplasmic dynein 1 is used by eukaryotic cells for minus-end directed microtubule-based transport of cargo. One such cargo is Rab7, a late endosomal marker. The purpose of this study is to identify the effects of this mutation on the transport of GFP-tagged Rab7 cargo in neurons from wild type (HH), heterozygous mutant (HR), and homozygous mutant (RR) mice harboring a *DYNC1HI* His306Arg mutation. Mouse embryos were euthanized, dissected to collect the hippocampal and cortical brain tissues, and these tissues were digested to isolate neurons. Nucleofection was used to introduce the exogenous GFP-Rab7 gene construct. These neurons were plated and imaged at 10 days *in vitro* using wide-field epifluorescence microscopy to generate image stacks of fluorescent GFP-Rab7 vesicles. Kymograph analysis was performed on the image stacks using MetaMorph software to measure several characteristics of movement. Statistical analysis of the data from each of the three genotypes shows there is no significant difference in Rab-7 transport between the three genotypes.

Table of Contents

Table of Figures

Introduction

Dynein

The dynein family is a group of motor proteins that are subdivided based on which of nine major classes of heavy chain the protein complex is built around [1]. The dynein heavy chain is composed of a motor domain belonging to the AAA+ ATPase superfamily and a tail domain that associates with various subunits, adaptor proteins, and cargo [1]. Cytoplasmic dynein 1, often referred to as cytoplasmic dynein or simply dynein, is used by eukaryotic cells for minus-end directed microtubule-based transport. The other classes of dynein play a role in the beating of cilia and transport of material in cilia and flagella. Dynein typically works opposite the kinesin family of motor proteins that are used in plus-end directed microtubule-based transport.

Cytoplasmic dynein is a two-headed motor assembled from dimers of cytoplasmic dynein 1 heavy chains (encoded by *DYNC1H1* in humans), intermediate chains, light-intermediate chains, and three different light chains [1]. Additionally, the regulators lissenecephaly 1 (LIS1), nuclear distribution E (NUDE), and the dynactin complex are involved in the majority of dynein's cellular functions [1]. These functions include the transport of vesicles and organelles such as endosomes and mitochondria, the transport of centrosome components, and the transport of transcription factors. Anchored dynein can pull the cytoskeleton to the edge of migrating cells such as neurons and is responsible for anchoring the Golgi and nuclear envelope to the cytoskeleton. In cell division, dynein helps assemble the mitotic spindle and is a part of the mechanism used to ensure correct spindle attachment and chromosome separation.

Dynein generates force through the hydrolysis of ATP. ATP binding, hydrolysis, inorganic phosphate release, and ADP release are each coupled to a structural change in the motor domain [1]. Dynein moves along microtubules, cytoskeletal filaments polymerized from α- and β-tubulin dimers. In most cells, the plus ends of microtubules are directed toward the cell periphery while the minus ends are directed toward the cell center. Cytoplasmic dynein dimers move between 8 and 16 nm per step along microtubule tracks. The average run length of dynein is approximately 1 μm [2-4], and the average velocity is slightly above 0.5 μm/s [2, 3].

Rab-7

Another important class of proteins in trafficking are Rab proteins. Rab proteins are GTPases (proteins that alternate between active and inactive forms based on GTP binding and hydrolysis) that belong to the Ras-like GTPase superfamily [5]. Rab proteins localize to specific intracellular compartments where they interact with effector proteins to regulate a variety of downstream functions. Rab7 is a Rab protein with several functions in mammalian cells. In endocytosis, Rab7 is a late endosomal marker, is involved in the biogenesis and maintenance of lysosomes, and regulates the pH of both late endosomes and lysosomes. Specifically in phagocytosis and macroautophagy, Rab7 is required for the fusion of phagosomes with late endosomes and lysosomes and autophagosomes with lysosomes [5]. Rab7 plays an additional role in the retrograde pathway used to recycle receptors. The retromer is a multisubunit complex that regulates retrograde transport from endosomes to the trans-Golgi network. Through interaction with the retromer's core complex and cargo recognition complex, Rab7 recruits the retromer to late endosomes. In all of these processes, Rab7 regulates organelle movement by recruiting effector proteins that anchor Rab7-positive vesicles and compartments to kinesin and

the dynein-dynactin complex. In addition to Rab7's general functions, it has specific functions in neurons. Rab7 controls endosomal trafficking and signaling of the nerve growth factor TrkA, plays a role in neurite outgrowth, helps regulate long-range axonal retrograde transport in motor neurons, and influences neuronal migration and dendrite morphology [5]. Charcot-Marie-Tooth (CMT) type 2 can be caused by mutations in the Rab7 gene, specifically CMT type 2B [6].

Charcot-Marie-Tooth

Charcot-Marie-Tooth is a neuromuscular disorder resulting from a wide variety of genetic mutations. CMT has a prevalence of approximately 1 in 2500 people, making it the most common hereditary neuromuscular disorder [6]. While each CMT mutation affects a different pathway, they all ultimately lead to axonal degeneration and the common phenotype seen in CMT patients. Symptoms include high arches, hammer toes, muscle weakness and wasting, sensory loss primarily in the feet and hands, and skeletal deformities, particularly in the feet.

CMT is classified into several types based on nerve pathology and mode of inheritance and sub-classified based on the causative gene. CMT type 1 (CMT1) is an autosomal dominant, demyelinating form. CMT1A is the most common of all CMT types and results from the over expression or (rarely) point mutations in the gene encoding the peripheral myelin protein 22 [6]. Demyelinating CMT that is autosomal recessive is classified as CMT4 and is more severe than the dominant form. Non-demylinating or axonal CMT is classified as type 2 (CMT2). Additional types include X-linked CMT (CMTX), dominant-intermediate CMT, CMT5, CMT6, and CMT3 (used to describe Dejerine-Sottas neuropathy, the most severe form of demyelinating CMT). Due to the genetic heterogeneity of CMT, it can be difficult to determine a patient's exact subtype. Diagnosis requires identifying a patient's type, taking a family history to determine the

inheritance pattern, and targeted genetic tests based on the genes most frequently associated with that type and pattern [6]. There is no cure or drug treatment for CMT (though ascorbic acid is in clinical trials in multiple countries); treatment is supportive and includes rehabilitative therapy, orthotics, shoe-modifications, and surgical treatment, such as tendon transfers to recover thumb function and scoliosis intervention.

Dynein Mutations and Transport Defects

Dynein is essential for the proper growth and function of neurons. In larval segmental nerves from Drosophila, reducing the amount of dynein had significant effects both on neuronal growth and vesicle transport [7]. When dynein was reduced by 50%, neurite projection length and cell body growth were reduced compared to 100% dynein levels. The growth rate of axons was also decreased from 1.80 μm/h to 0.62 μm/h at 50% dynein levels. In vesicular transport, both retrograde and anterograde vesicle transport velocities were significantly reduced, the number of stalled vesicles increased, and the number of reversing vesicles decreased [7]. These changes in vesicle transport may contribute to the growth defects seen when dynein is reduced.

In the filamentous fungus *Aspergillus nidulans*, mutations in dynein can result in defects in organelle positioning and velocity [8]. Mutations in the AAA+ domain (G1937C, R2795L) result in the increased accumulation of endosomes and peroxisomes in the hyphal tips, similar to what is seen in the strain lacking dynein; however in contrast to that strain, AAA+ domain mutants do not show differences in the position of the nucleus. When introduced to the *Saccharomyces cerevisiae* dynein motor domain, these the G1937C and R2795L mutations resulted in a 66% and 98% reduction in velocity respectively [8].

Defects in axonal transport are associated with a number of human neuropathies including amyotrophic lateral sclerosis (ALS), frontotemporal dementia (FTD), axonal forms of CMT, and spinal muscular atrophy (SMA) [9]. These defects can have several different causes and involve different components of the transport machinery. Genetic mutations, one such cause, include downregulated mRNA of dynactin-1 in sporadic ALS patients, kinesin mutations in spastic paraplegia, schizophrenia, and CMT2A, and dynein mutations in CMT2O and possibly Huntington's disease. Other causes of axonal transport defects include mitochondrial oxidative stress, as seen in mouse models of Alzheimer's disease (AD) and ALS, and post translational changes to proteins that make up the transport machinery, such as the alterations to microtubule-associated proteins that are associated with AD and FTD.

Mutant Dynein Mouse Models

Three mutant dynein mouse models have been used to characterize dyneinopathies. The *Legs at odd angles (Loa)* mutation is a F580Y autosomal dominant mutation that results in progressive muscle loss and decline in locomotor ability (in heterozygous mice) [10]. This phenotype is also seen in the *Cramping* 1 (*Cra1)* mutation, a Y1055C mutation [10]. Mice that are homozygous for either mutation are unable to move and die shortly after birth. When compared to wild-type littermates, homozygous *Cra1* and *Loa* embryos show a reduction in embryonic spinal anterior horn cells (AHC), increased apoptosis in AHCs, and protein depositions similar to those seen in human ALS. In spinal cord neurons, cells that were homozygous for the *Loa* mutation show a reduction in the frequency of high speed retrograde transport and an increase in stationary pauses when compared to wild-type neurons. A third mutation, *Sprawling* (*Swl),* is a nine base pair deletion at DYNC1H1 residues 1040-1043 [11].

Heterozygous *Swl* mice have normal peripheral motor nerve function but show a defect in proprioceptive sensory neurons. This defect was found to be common to heterozygous *Loa* mice. These mutations are located in the homodimerization domain of the cytoplasmic dynein 1 heavy chain.

The *Loa* mutation's effects on motor processivity and neuronal migration have been further characterized in *in vitro* and *in vivo* studies. Purified Loa/+ dynein has decreased affinity for microtubules during ATP hydrolysis but not in the absence of ATP during the strong microtubule binding state, compared to wild type dynein [12]. The run lengths of purified Loa/+ and Loa/Loa were reduced by 23% and approximately 50% respectively compared to wild type dynein. Reduced run lengths by Loa/+ and Loa/Loa were also seen *in vivo* analysis of late endosome/lysosome motility, as well as a decrease in overall average velocity; instantaneous velocity was unchanged. These results suggest that the *Loa* mutation impairs coordination between the two motor domains and that this results in decreased dynein run length, which would more strongly affect long cells such as motor and sensory neurons.

The *Loa* mutation also affects neuronal migration in mice. Compared to wild-type brains, Loa/Loa brains had a disorganized cortex and a smaller, more compact a dentate gyrus in the hippocampus [13]. Loa/Loa brains also show neuronal migration defects; migration to the cortical plate of the brain was delayed by 2 days in mutant mice. Migration delays can be seen in Loa/Loa neurons using live cell imaging, where mutant neurons showed a reduced rate of somal translocation and remained in their elongated, migrating shape for a longer time period compared to wild-type neurons. As mutant dynein was still able to bind its regulatory proteins, the *Loa* mutation's effect on brain organization and neuronal migration are likely due to the mechanochemical defects the mutation causes.

The effects of the *Loa* mutation on dynein function have also been studied in *Neurospora crassa*, an organism in which dynein is nonessential. In *N. crassa*, mutant *Loa* dynein showed reduced localization at hyphal tips and altered localization to spherical organelles in comparison to wild-type dynein [14]. Vesicle motility was only slightly altered in the *Loa* strain compared to the wild-type; *Loa* strains showed a statistically significant decrease in inward velocity, inward distance traveled, and outward velocity, but other differences were not significant.

Dynein Mutations in Neuropathies

The first dynein mutation found in humans that caused disease was a *DYNC1H1* p.His306Arg, meaning that the histidine that is normally found at the 306 position in the dynein heavy chain is converted to an arginine due to this mutation. This residue is a highly conserved part of the heavy chain's homodimerization domain. This mutation was found to cause CMT2 in humans and was first described by Weedon *et al.* in 2011 [15]. They studied a large family with many members affected by CMT2. After inheritance patterns and sequencing eliminated the most common pathogenic mutations associated with CMT2, whole-exome sequencing of three affected individuals revealed they all shared the p.His306Arg *DYNC1H1* missense mutation [15]. This mutation was shared by other members of the family and was not found in control chromosomes. This subtype was designated CMT2O. In 2012, a second family (two siblings and their mother) was found to have this same mutation; however the two affected siblings presented with spinal muscular atrophy with lower extremity predominance (SMA-LED) [16]. This demonstrates the multiple pathogenic effects this mutation can have. The mouse line that was used the current study harbors this mutation and so is a mouse model for CMT-based neuropathies

Since the publication of the first dynein mutation, additional dynein mutations have been linked to a variety of other neuropathies. Two *de novo* missense mutations in this gene have been identified in patients with severe intellectual disability [17]. The first, p.His3822Pro, is located in the motor domain of the heavy chain. The patient with this mutation exhibited developmental delays, mild facial dysmorphism, and signs of brain malformation. The second mutation, p.Glu1518Lys, is located in the C-terminal stem domain, outside of the homodimerization region. The patient with this mutation exhibited both severe intellectual disability and severe neuronal migration defects. A CT scan of the patient showed clear signs of cortical malformation. Mutations in the tail domain of *DYNC1H1* have been shown to cause spinal muscular atrophy with lower extremity predominance (SMA-LED) [18]. Three different missense mutations (I584L, K671E, and Y970C) result in similar phenotypes: leg weakness and muscle atrophy beginning in childhood and motor neuron disease without sensory involvement. Notably, the patient with the Y970C mutation also showed some cognitive impairment. Further research has only expanded the number of *DYNC1H1* mutations associated with SMA-LED. In a study of thirty SMA patients with *DYNC1H1* mutations, researchers found 8 novel tail domain and 2 novel motor domain mutations, with twenty-three of the thirty cases demonstrating autosomal dominant inheritance [19]. Cognitive impairments were also seen in nine of the thirty patients in this study, many of whom had additional ADHD traits. A tenth patient showed normal cognitive ability but was diagnosed with ADHD. These rates are higher than those of the general population and were not associated with the severity of the patient's motor impairment. Cortical malformation was seen in four of the nine cognitively impaired patients that underwent an MRI.

Rational

While it is clear that dynein mutations are linked to neuropathies, the mechanism by which these mutations cause human disease is unknown. The primary question is: Why do dynein heavy chain mutations cause neurodegenerative diseases when dynein is essential in every cell of the body? This effect may be due to impaired processivity of dynein resulting from the disruption of microtubule binding or subunit association (proposed by Ori-McKenney *et al.* [12] for *Loa* mice, for example) or due to disrupted cargo binding. My hypothesis is that the *DYNC1H1* His306Arg mutation interferes with the transport of cargo in some cell types. I tested this hypothesis by measuring GFP-Rab7 transport in embryonic cortical neurons from three genotypes of mice (HH, HR, and RR).

Primary cells from a mutant mouse line were used because primary cells more closely mimic what happens *in vivo*, compared to an immortalized cell line that has multiple other mutations that allow it to continuously divide or an *in vitro* system using purified dynein that lacks other factors that important in cells. The King lab had previously developed a mouse line that harbors the *DYNC1H1* His306Arg mutation, so primary cells were readily available. Additionally, other studies investigating the effects of dynein heavy chain mutations used mouse models. This allows comparison between the effects of a naturally occurring human mutation and artificially created mouse mutations.

Cortical neurons were chosen because previous studies had shown cortical malformation in humans [17, 19] and neuronal migration defects in mice [13]. Additionally, cortical neurons are a well described experimental system and members of the King laboratory have training in mouse brain dissections. Embryonic neurons were used because they are easier to isolate, culture, and nucleofect compared to adult neurons. Also, we do see differences in cortical

development even at early time points and experimental conditions were easier to optimize as we did not have to wait as long between trial and the next.

Rab7 was chosen as a cargo for several reasons. Previous studies had shown that dynein motor domain mutations can cause altered positioning of endosome and peroxisomes [8] while dynein heavy chain mutations can cause altered late endosome/lysosome transport [12]. Rab7 is a late endosome marker and so a change in the interaction between dynein and Rab7 due to the *DYNC1H1* His306Arg mutation would likely cause altered late endosome transport similar to what is seen in other mouse models. Additionally, GFP-Rab7 is a readily available construct and is an established cargo for motility studies.

Materials and Methods

The overall goal of my research was to compare the transport of Rab7 cargo in neurons from three different genotypes of mice. The neurons used for this study came from an established line of mice housed at the transgenic animal facility at the Burnett Biomedical Sciences Building (IACUC protocol 15-31). They include wild-type (HH), heterozygous mutant (HR), and homozygous mutant (RR) mice. These mutant mice harbor a *DYNC1H1* His306Arg mutation. To collect neurons, heterozygous animals were mated and the embryos euthanized at day 16.5. These embryos were dissected to collect the cortex of their brains. This region was used as neurons from the cortex can be easily isolated and is a well-studied experimental system. Embryonic cortical neurons are also easier to grow and transfect compared to adult neurons. Additionally, other dynein mutations are linked to cortical malformation and the H306R mutant mouse line shows cortical disorganization at early time points. A tail snip from each embryo was also taken in parallel for use in genotyping individual animals. Genomic DNA was extracted from the tail tissue using a Norgen Genomic DNA Isolation Kit (#24700, #24750), amplified with specific primers using PCR, and run on an agarose gel to determine each mouse's genotype based on a specific band pattern. The cortical tissue was digested to isolate neurons. Nucleofection was used to introduce the exogenous GFP-Rab7 gene construct that will generate fluorescent tagged Rab7 positive vesicles in the neurons. GFP-Rab7 is easily available and previous studies of the effects of dynein mutations on motility used late endosomes/lysosomes; this makes GFP-Rab7 a good cargo to track. After nucleofection, these neurons were plated at an appropriate density on poly-D lysine (0.3µg/mL) coated sterile glass coverslips. Preliminary studies showed that 10 days in vitro (DIV) produced the healthiest neurons and stronger GFP signals when compared to other time points.

After 10 DIV, each coverslip was imaged using wide-field epifluorescence microscopy utilizing a search-and-rescue pattern to avoid duplications. Neurons that were used for the production of movies were identified one of two ways, depending on the condition of the coverslip. The first way was using DIC optics to identify healthy neurons and then switching to the green channel to confirm if the cell took up the GFP-Rab7 construct. The second way was using the green channel to identify bright signals and then DIC optics to confirm that the signal is a healthy neuron. In the case of an ambiguous signal, the red and blue channels were used to identify if it is a true signal from GFP-Rab7 or autofluorescence (Figure 1).

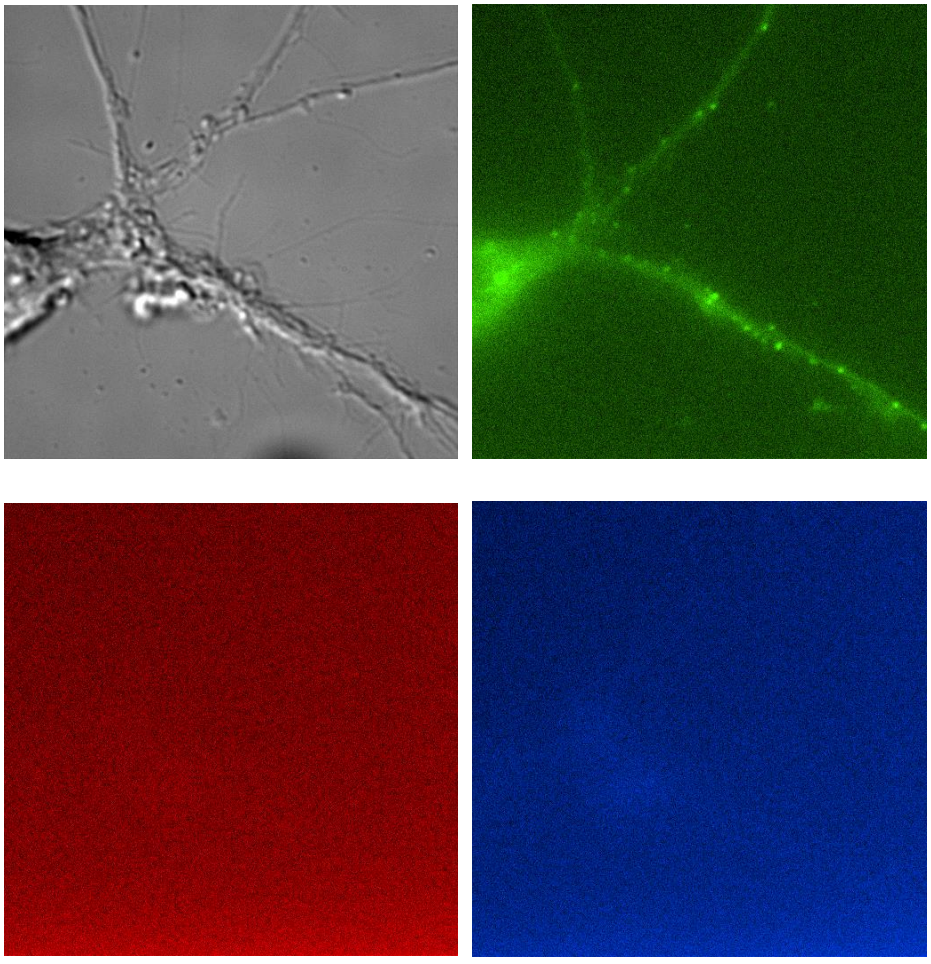

Figure 1 Top Left: DIC Optics image of a cortical neuron. Top Right: Image of the same cortical neuron in the green channel. Bottom: Images of the same cortical neuron in the red and blue channels. The absence of fluorescence in these channels confirms that the signal shown in the green channel is due to the expression of GFP-Rab7.

To create an image stack for a neuron, the cell body was placed at a far corner of the field of view to maximize the space for the neuronal process. We used 100x magnification with an additional 1.5x adaptor, bringing the total magnification to 150x. Images were obtained at 10 frames per second (fps) for 50 seconds yielding an image stack with 500 frames. Still images were then captured of the process and of the cell body, in both the green and DIC channels. Image stacks were converted to monochrome images and inverted to improve the visibility of motility events (Figure 2).

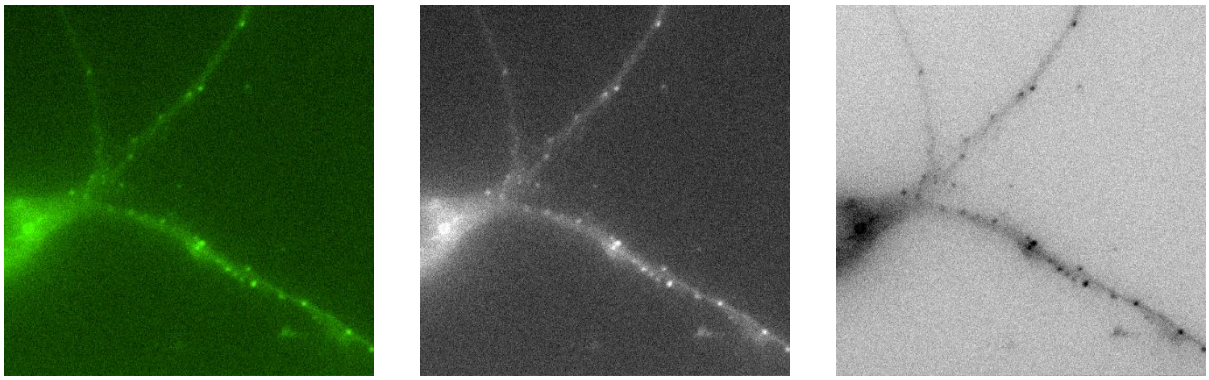

Figure 2 Left: Original Image. Center: Original image converted to monochrome. Right: Monochrome image with the colors inverted.

Kymograph analysis was performed on the image stacks using MetaMorph software. Kymographs are graphical representations of movement over time. To generate a kymograph, the image stack was opened in MetaMorph software and a region line was drawn that extended the entire length of the neuronal process, beginning near the cell body and extending to the end. This line was expanded to cover the entire width of the process (Figure 3).

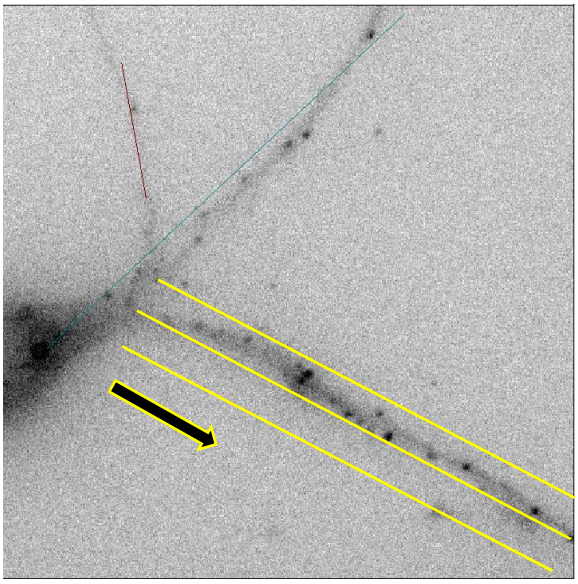

Figure 3 Region lines on an image stack. The active region is in yellow, with the yellow and black arrow representing the direction the region was drawn in

The kymograph function in MetaMetamoph will generate a kymograph for only the active region. The kymograph function will sum up the intensity of the signal across the width of the line for each point along the length of the region line. This will be plotted as a single row of pixels (Figure 4).

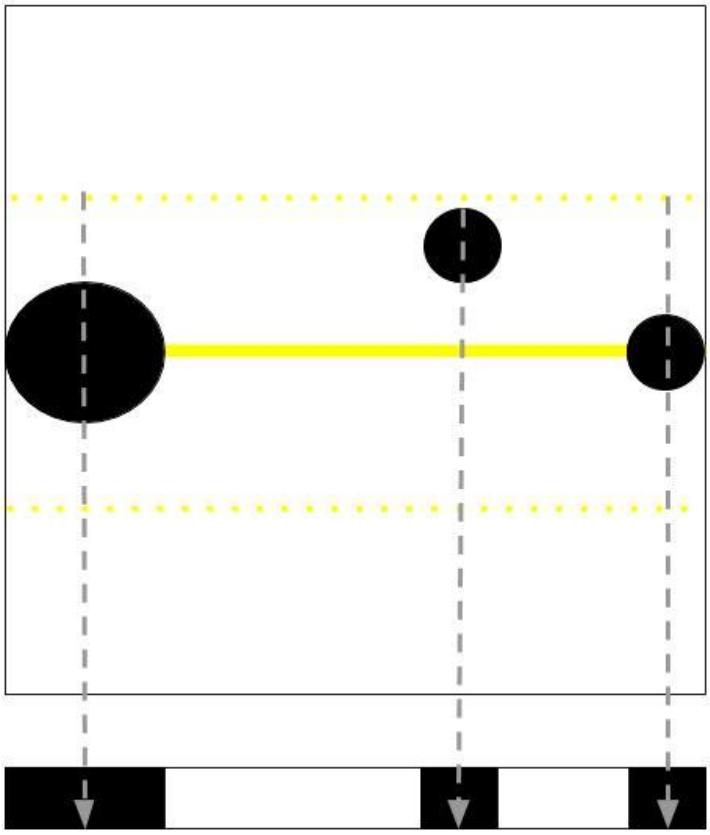

Figure 4 Schematic of summing intensities. The solid yellow line represents the region line while the dotted yellow lines represent the expansion of the line to cover the width of the process. The black dots represent vesicles of various sizes. The bottom row represents the result of summing the intensities from one dotted yellow line to the other, for the length of the region line. The large vesicle creates a large, solid row of pixels while the smaller vesicles create smaller ones. The positions of the darkened pixels correspond to the vesicle's location along the region line

The process of summing intensities was repeated for each frame of the image stack, generating an image 500 pixels tall where each frame is represented by a single row of pixels. This vertical axis corresponds to time, where a change from one pixel to another, the same as one frame to another, is equivalent to a change of 1/10th of a second.

A signal from a vesicle will appear on the image stack as a black circle (Figure 2 Right). When summed and plotted in a kymograph, that signal will be represented as several black pixels in a row, the number of which depends on the size of the vesicle (Figure 4). If the vesicle moves during the 1/10th of a second between one frame and the next, its position and signal along the

region line will shift. In this case, the row of black pixels that represent the vesicle on the kymograph will be in a different location in the next row of pixels. If the vesicle continues moving for multiple frames, the horizontal position of the dark pixels representing the vesicle on the kymograph will continue to shift between each row. This will create a diagonal line where the width of the line represents the distance traveled and the height of the line is the number of frames it took to move that distance, which can be converted to seconds. Stationary vesicles will create a signal that does not change places over time; therefore each row of pixels in the kymograph will have the darkened pixels representing the vesicle in the same place. This creates a straight line (Figure 5, 6)

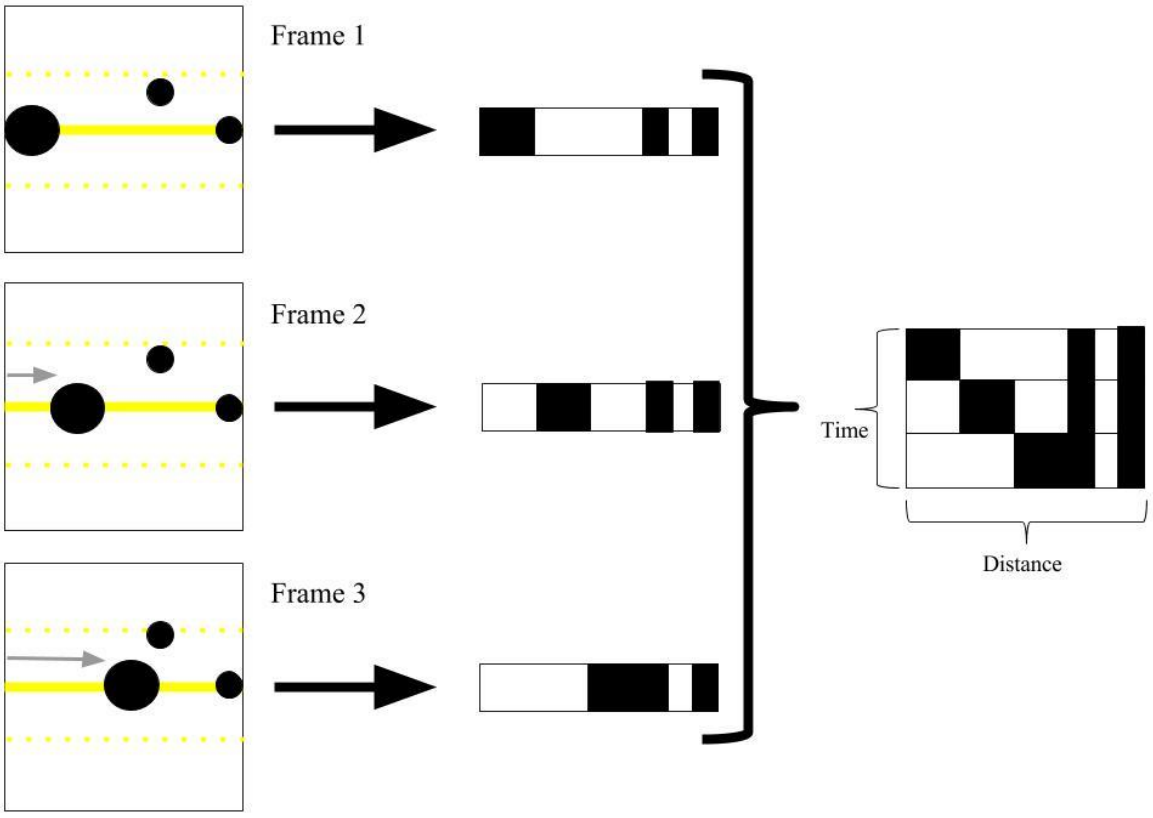

Figure 5 Schematic of the kymograph generation process with a moving vesicle. The solid yellow line represents the region line while the dotted yellow lines represent the expansion of the line to cover the width of the process. The black dots represent vesicles of various sizes.

Each frame yields the bar to the right as a result of summing the intensities from one dotted yellow line to the other, for the length of the region line. The large vesicle creates a large, solid row of pixels while the smaller vesicles create smaller ones. The positions of the darkened pixels correspond to the vesicle's location along the region line. As the large black vesicle is moving, its signal shifts between one frame and the next, which causes the line of pixels representing it to shift.

When the bars representing the row of pixels generated from summing intensities are plotted one after the other, it creates the graph to the right. The large, moving vesicle's signal creates a diagonal line while the two small, stationary vesicles create a straight line.

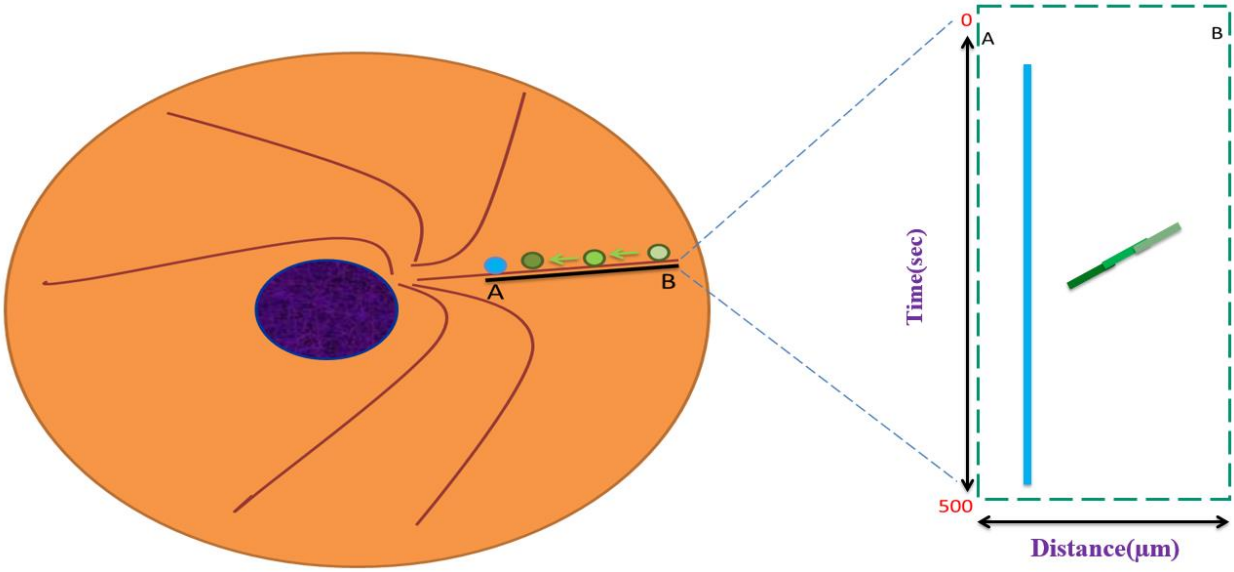

Figure 6 Schematic of a kymograph generated from movements in a cell (Provided by Dr. Stephen King). The green circles represents a single vesicle in motion along a microtubule while the blue circle represents a single stationary vesicle. A region line drawn from point A to point B will generate the kymograph to the right, where the vesicles closest to point A will be on the left and the vesicles closest to point B are on the right.

After generating a kymograph (Figure 7 Left) for the active region (Figure 3), each line was traced with a region line where it deviated from a straight path, starting from the top (Figure 7 Right). Straight lines represent stationary bodies.

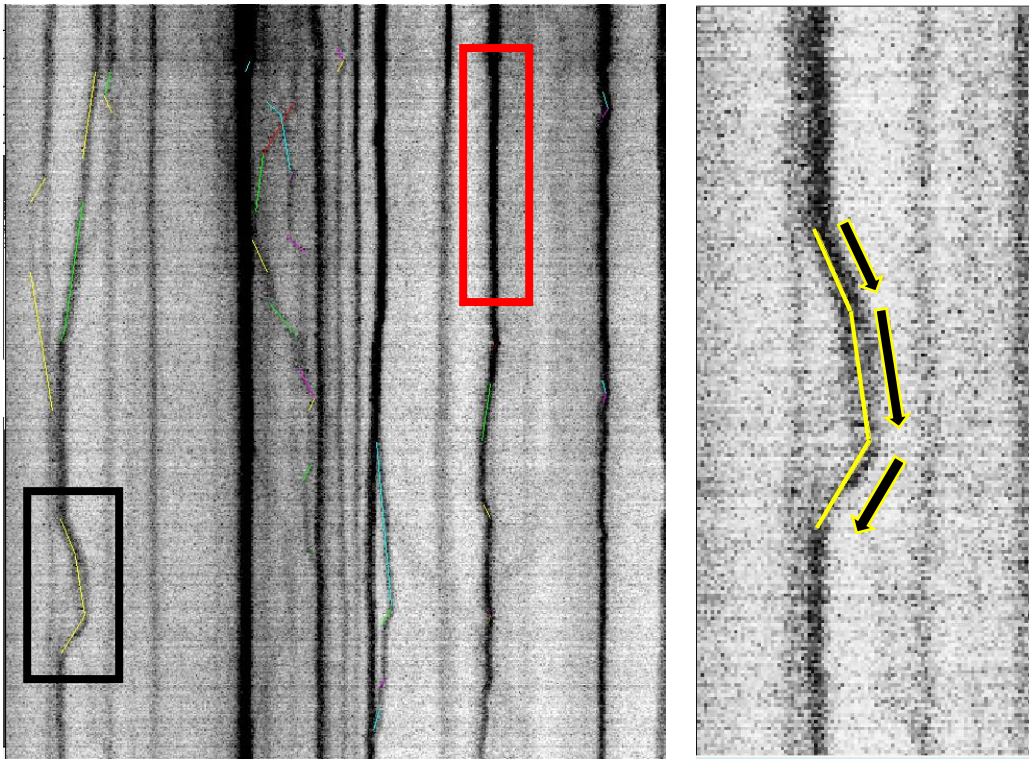

Figure 7: Left: kymograph generated from the active region shown in Figure3. An example of a stationary body is boxed in red. Right: Magnification of the region boxed in black showing motility events. The direction of the region lines is represented by the black and yellow arrows.

Region data (width, height, and angle) were logged in a Dynamic Data Exchange file, which created an Excel file linked to the Metamorph software. This data was then entered into a formula sheet generated by the King lab that calculated distance in microns, time in seconds, and directionality (in or out with respect to the cell body) using previously established conversion factors (Appendix). Average distance and velocity, standard deviations, and number of motility events were calculated for each genotype in both the inwards and outwards directions. Statistical analysis was performed using one-way ANOVA and Bonferroni's multiple comparisons test in GraphPad to compare the velocity and distances traveled of each genotype. Bar graphs were generated in Microsoft PowerPoint and scatterplots were generated in KaleidaGraph.

Results

The goal of this study was to compare the transport of Rab7 cargo in neurons from three different genotypes of mice. My hypothesis was that the *DYNC1H1* His306Arg mutation interferes with the transport of cargo in some cell types. I tested this hypothesis by measuring GFP-Rab7 transport in embryonic cortical neurons from three genotypes of mice (HH, HR, and RR). Primary cells from our mutant mouse line served as an experimental system that more closely mimicked what is seen *in vivo*. Embryonic cortical neurons were chosen because of the brain malformation seen in previous studies [13, 17, 19] and because embryonic neurons are easier to isolate, culture, and nucleofect. Rab7 was used as a cargo because of its role as a late endosome marker and its wide availability.

This study included 39 cells: 15 HH, 14 HR and 10 RR. No qualitative difference in nucleofection rates and GRP-Rab7 expression was seen between genotypes (Figure 8).

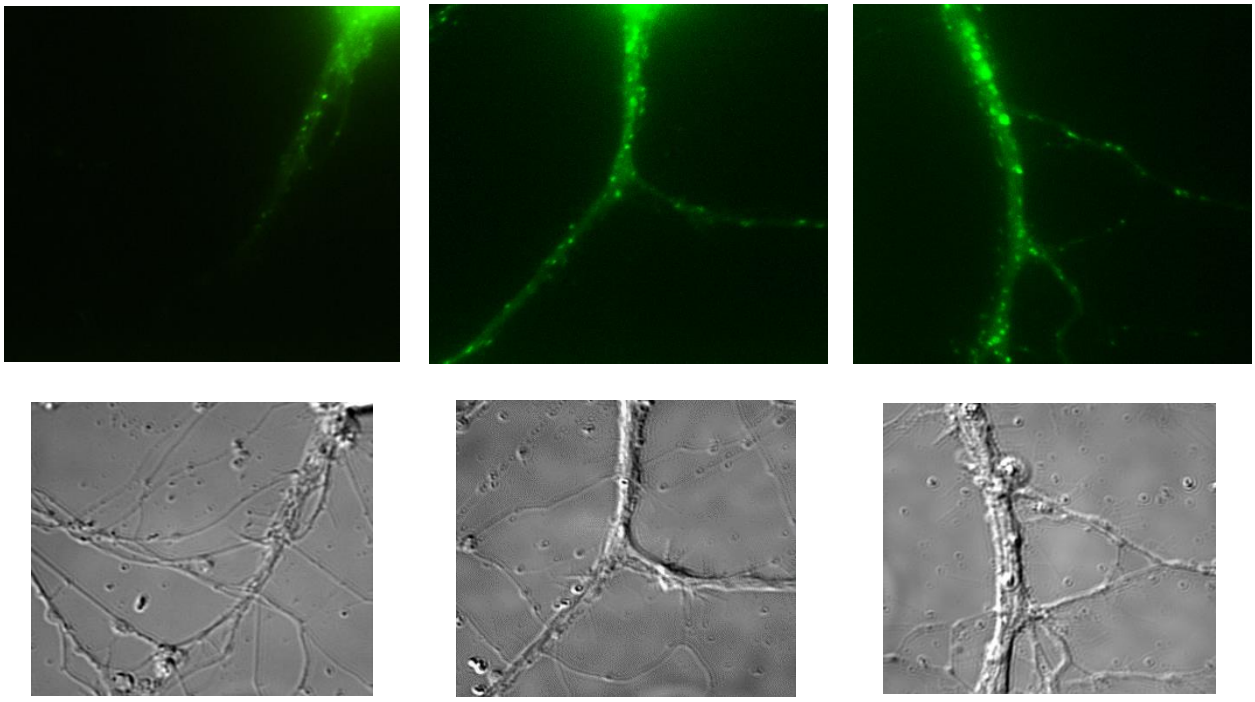

Figure 8 Comparison of neurons between genotypes (150x)

The 15 HH cells had 231 movements, the 14 HR cells had 322 movements, and the 10 RR cells had 202 movements. Each genotype had slightly more inwards movements than outwards movements (Figure 9).

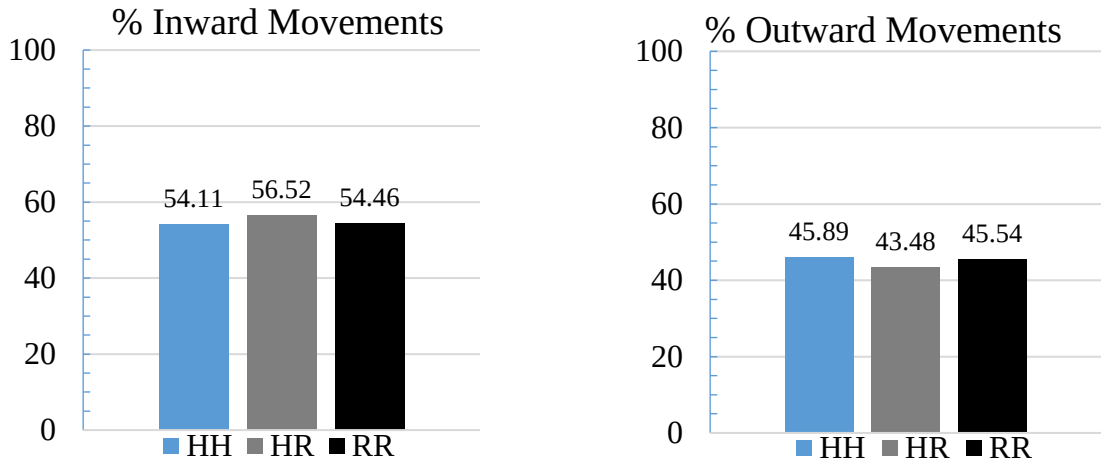

Figure 9 Number of inwards and outwards movements as a percent of total movements by genotype. Percent of inwards movements range from 54.11% to 56.52%. Percent of outwards movements range from 43.48% to 45.89%.

In the inwards direction, there was not a significant difference between genotypes in either distance (p-value: 0.5703; Figure 10) or velocity (p-value 0.963; Figure 11) using one-way ANOVA. Bonferroni's multiple comparisons test showed there was no significant difference between any genotype pairs.

A

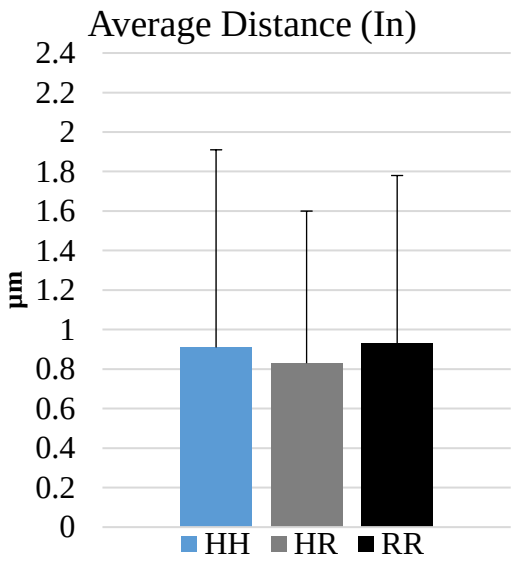

B

	HH	HR	RR
n (cells)	15	14	10
NUMBER OF MOVEMENTS	125	182	110
AVERAGE (µm)	0.91	0.83	0.93
STANDARD DEVIATION	1.00	0.77	0.85

C

Genotype	P-value	Significance?
HHvsHR	> 0.9999	Not significant
HHvsRR	> 0.9999	Not significant
HRvsRR	> 0.9999	Not significant

Figure 10A: Average distance traveled in the inwards direction in µm. B: Average distance traveled in the inwards direction, standard deviation, and number of movements in the inwards direction by genotype. C: Results of Bonferroni's multiple comparisons test.

A

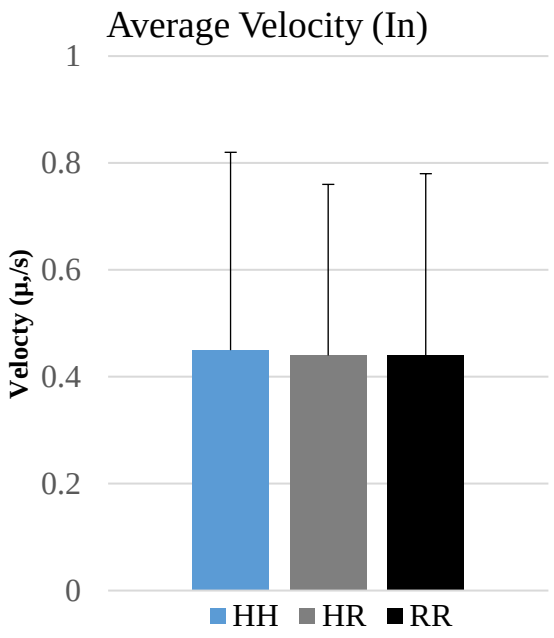

B

	HH	HR	RR
n (cells)	15	14	10
NUMBER OF MOVEMENTS	125	182	110
AVERAGE (µm/s)	0.45	0.44	0.44
STDEV	0.37	0.32	0.34

C

Genotype	P-value	Significance?
HHvsHR	> 0.9999	Not significant
HHvsRR	> 0.9999	Not significant
HRvsRR	> 0.9999	Not significant

Figure 11A: Average velocity in µm/s in the inwards direction in µm. B: Average velocity in the inwards direction, standard deviation, and number of movements in the inwards direction by genotype. C: Results of Bonferroni's multiple comparisons test.

In the outwards direction, there was not a significant difference between genotypes in either distance (p-value: 0.0507; Figure 12) or velocity (p-value 0.1482; Figure 13) using one-way ANOVA. Bonferroni's multiple comparisons test showed there was no significant difference between any genotype pairs. Neither the inwards or outwards direction showed any correlation between distance traveled and velocity (Fig. 14).

A

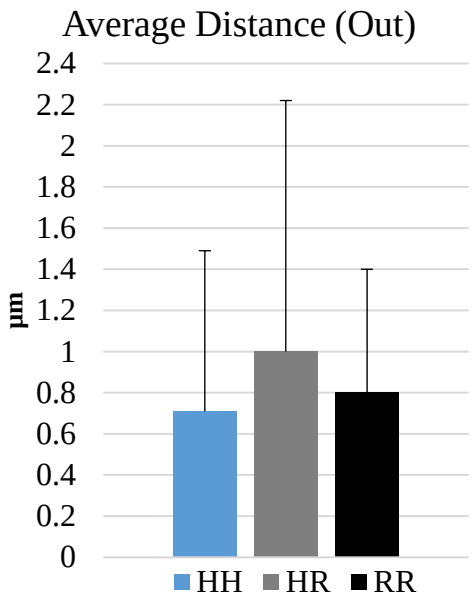

B

	HH	HR	RR
n (cells)	15	14	10
NUMBER OF MOVEMENTS	106	140	92
AVERAGE	0.71	1.00	0.80
STDEV	0.78	1.22	0.60

C

Genotype	P-value	Significance?
HHvsHR	0.0556	Not significant
HHvsRR	> 0.9999	Not significant
HRvsRR	0.3552	Not significant

Figure 12 A: Average distance traveled in the outwards direction in µm. B: Average distance traveled in the outwards direction, standard deviation, and number of movements in the inwards direction by genotype. C: Results of Bonferroni's multiple comparisons test.

A

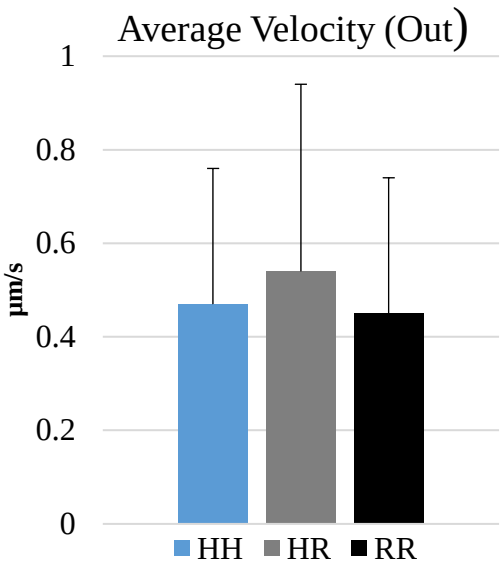

B

	HH	HR	RR
n (cells)	15	14	10
NUMBER OF MOVEMETNS	106	140	92
AVERAGE	0.47	0.54	0.45
STDEV	0.29	0.40	0.29

C

Genotype	P-value	Significance?
HHvsHR	0.3322	Not significant
HHvsRR	> 0.9999	Not significant
HRvsRR	0.1482	Not significant

Figure 13 A: Average velocity in µm/s in the outwards direction in µm. B: Average velocity in the outwards direction, standard deviation, and number of movements in the inwards direction by genotype. C: Results of Bonferroni's multiple comparisons test.

A

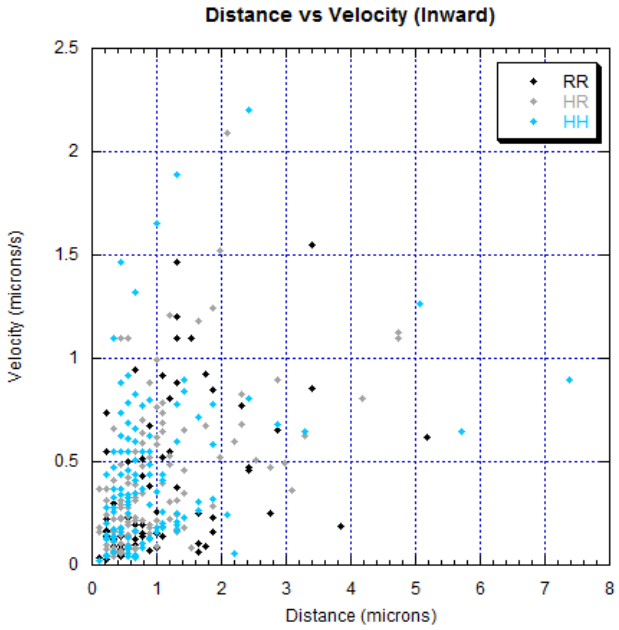

B

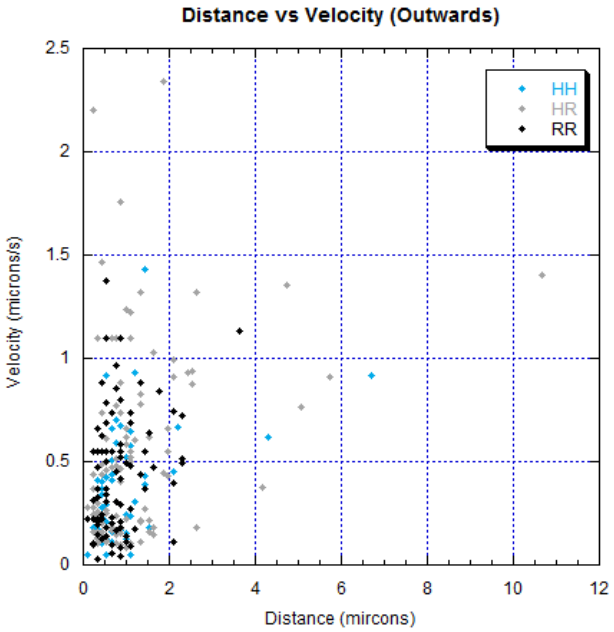

Figure 14 A: Scatterplot of distance vs velocity in the inwards direction showing all three genotypes. There is no correlation between velocity and distance, or any clustering of genotypes representing a pattern of movement, for example fast but short movements. B: Scatterplot of distance vs velocity in the outwards direction showing all three genotypes. There is no correlation between velocity and distance, or any clustering of genotypes representing a pattern of movement.

Discussion

The mechanism by which dynein mutations cause neuropathies in humans is unknown, as is the reason dynein mutations have not been found to affect other systems. We hypothesized that the DYNC1H1 His306Arg mutation may result in altered intracellular motility in neurons, possibly contributing to the mutation's pathology. Overall, my experiments do not support the hypothesis as there was not a difference in intracellular motility of GFP-Rab7 vesicles between wild type, heterozygous mutant, and homozygous mutant embryonic mouse neurons. In both the inwards and outwards directions, distance traveled and velocity were not significantly different. The averages for both distance and velocity were similar to what had previously been observed for cytoplasmic dynein [2-4]. Additionally, there was no correlation between distance traveled and velocity and there was no clustering of genotypes. Therefore, it seems that no genotype is prone to characteristic movement patterns, such as short and slow moments or movements that are intermediate in both speed and distance traveled. Overall motility patters were similar to what had previously been observed [2].

Other studies have shown that dynein mutations can alter intracellular motility [10, 12, 14]; for example, *Loa* mice showed transport defects in spinal column neurons [10]. However, based on these results the DYNC1H1 His306Arg mutation does not interfere with dynein's ability to interact with Rab7 and its effector proteins, with microtubule binding, or with motor domain coordination, unlike what was seen in other studies [12]. This difference may be because the DYNC1H1 His306Arg seems to be a less severe mutation, as homozygous mutant mice are viable, unlike *Loa* and *Cra1* homozygous mice [10].

Additional studies using alternative cargos and neuron types may yield differing results. The DYNC1H1 His306Arg mutation likely does have some effect on neurons; DYNC1H1

His306Arg mutant mice do show a neuromuscular disorder phenotype similar to that of other mutant dynein mouse models [10] and brain malformation, which is also seen in the *Loa* mouse [13] and other human dynein mutations [17, 19]. In the case of the DYNC1H1 His306Arg mutation, motor and sensory neurons may show results more consistent with other studies as these neuron types are affected most by CMTO2. Alternative, more neuronal specific cargo may also show different results. For example, vascular endothelial growth factor A (VEGF-A) is a neurotrophic factor that promotes neuron survival in multiple neurodegenerative diseases [20]; deletion of the hypoxia-response element of VEGF-A resulted in lower motor neuron degeneration similar to that of ALS [21]. These alternatives would further test the hypothesis. Alternative hypotheses could be tested using biochemical methods to determine the mutant dynein heavy chain's affinity for other subunits, effector proteins, and cargo. Future directions include analyzing alternative cargoes and neuron types to continue investigating the mechanism by which this dynein mutation causes disease.

References

1. Roberts, A.J., et al., *Functions and mechanics of dynein motor proteins.* Nat Rev Mol Cell Biol, 2013. **14**(11): p. 713-26.

2. King, S.J. and T.A. Schroer, *Dynactin increases the processivity of the cytoplasmic dynein motor.* Nat Cell Biol, 2000. **2**(1): p. 20-4.

3. Reck-Peterson, S.L., et al., *Single-molecule analysis of dynein processivity and stepping behavior.* Cell, 2006. **126**(2): p. 335-48.

4. Wang, Z., S. Khan, and M.P. Sheetz, *Single cytoplasmic dynein molecule movements: characterization and comparison with kinesin.* Biophys J, 1995. **69**(5): p. 2011-23.

5. Guerra, F. and C. Bucci, *Multiple Roles of the Small GTPase Rab7.* Cells, 2016. **5**(3).

6. Pareyson, D. and C. Marchesi, *Diagnosis, natural history, and management of Charcot-Marie-Tooth disease.* Lancet Neurol, 2009. **8**(7): p. 654-67.

7. Iacobucci, G.J., et al., *Spatial and temporal characteristics of normal and perturbed vesicle transport.* PLoS One, 2014. **9**(5): p. e97237.

8. Tan, K., et al., *A microscopy-based screen employing multiplex genome sequencing identifies cargo-specific requirements for dynein velocity.* Mol Biol Cell, 2014. **25**(5): p. 669-78.

9. Liu, X.A., V. Rizzo, and S.V. Puthanveettil, *Pathologies of Axonal Transport in Neurodegenerative Diseases.* Transl Neurosci, 2012. **3**(4): p. 355-372.

10. Hafezparast, M., et al., *Mutations in dynein link motor neuron degeneration to defects in retrograde transport.* Science, 2003. **300**(5620): p. 808-12.

11. Chen, X.J., et al., *Proprioceptive sensory neuropathy in mice with a mutation in the cytoplasmic Dynein heavy chain 1 gene.* J Neurosci, 2007. **27**(52): p. 14515-24.

12. Ori-McKenney, K.M., et al., *A cytoplasmic dynein tail mutation impairs motor processivity.* Nat Cell Biol, 2010. **12**(12): p. 1228-34.

13. Ori-McKenney, K.M. and R.B. Vallee, *Neuronal migration defects in the Loa dynein mutant mouse.* Neural Dev, 2011. **6**: p. 26.

14. Sivagurunathan, S., et al., *A mouse neurodegenerative dynein heavy chain mutation alters dynein motility and localization in Neurospora crassa.* Cytoskeleton (Hoboken), 2012. **69**(9): p. 613-24.

15. Weedon, M.N., et al., *Exome sequencing identifies a DYNC1H1 mutation in a large pedigree with dominant axonal Charcot-Marie-Tooth disease.* Am J Hum Genet, 2011. **89**(2): p. 308-12.

16. Tsurusaki, Y., et al., *A DYNC1H1 mutation causes a dominant spinal muscular atrophy with lower extremity predominance.* Neurogenetics, 2012. **13**(4): p. 327-32.

17. Willemsen, M.H., et al., *Mutations in DYNC1H1 cause severe intellectual disability with neuronal migration defects.* J Med Genet, 2012. **49**(3): p. 179-83.

18. Harms, M.B., et al., *Mutations in the tail domain of DYNC1H1 cause dominant spinal muscular atrophy.* Neurology, 2012. **78**(22): p. 1714-20.

19. Scoto, M., et al., *Novel mutations expand the clinical spectrum of DYNC1H1-associated spinal muscular atrophy.* Neurology, 2015. **84**(7): p. 668-79.

20. Stanojlovic, M., et al., *Inhibition of Vascular Endothelial Growth Factor Receptor 2 Exacerbates Loss of Lower Motor Neurons and Axons during Experimental Autoimmune Encephalomyelitis.* PLoS One, 2016. **11**(7): p. e0160158.

21. Oosthuyse, B., et al., *Deletion of the hypoxia-response element in the vascular endothelial growth factor promoter causes motor neuron degeneration.* Nat Genet, 2001. **28**(2): p. 131-8.

Appendix: Motility Data

HH

Real distance (µm)	Velocity (µm/s)	Directionality
0.44	0.73	IN
0.44	0.73	IN
2.42	2.20	IN
1.32	1.89	IN
0.44	0.88	IN
1.32	0.17	IN
2.09	0.25	IN
0.66	0.05	IN
1.65	0.27	IN
3.30	0.65	IN
2.42	0.81	IN
0.44	0.73	IN
0.55	0.25	IN
2.86	0.68	IN
0.88	0.29	IN
0.99	0.35	IN
0.55	0.09	IN
0.77	0.77	IN
5.72	0.64	IN
1.10	0.44	IN
1.87	0.58	IN
0.55	0.61	IN
0.33	0.55	IN
0.88	0.12	IN
1.87	0.32	IN
1.43	0.89	IN
1.32	0.19	IN
1.65	0.31	IN
0.77	0.11	IN
1.32	0.60	IN
0.66	0.05	IN
0.11	0.02	IN
0.33	1.10	IN
0.33	0.33	IN
0.66	0.51	IN

Real distance (µm)	Velocity (µm/s)	Directionality
0.44	0.63	IN
0.33	0.37	IN
0.33	0.55	IN
0.33	0.25	IN
1.87	0.78	IN
0.33	0.06	IN
0.55	0.06	IN
0.44	0.34	IN
0.88	0.13	IN
1.43	0.84	IN
0.66	0.17	IN
0.55	0.07	IN
0.55	0.46	IN
0.22	0.04	IN
0.22	0.44	IN
0.88	0.55	IN
0.22	0.13	IN
0.55	0.04	IN
1.10	0.41	IN
0.44	0.73	IN
0.55	0.31	IN
0.33	0.12	IN
0.77	0.08	IN
0.66	0.60	IN
0.55	0.79	IN
0.66	0.04	IN
0.22	0.20	IN
0.44	0.44	IN
1.10	0.20	IN
1.32	0.21	IN
0.66	0.44	IN
0.33	0.33	IN
0.33	0.28	IN
0.55	0.32	IN
0.22	0.15	IN

Real distance (µm)	Velocity (µm/s)	Directionality
0.44	0.16	IN
0.55	0.34	IN
0.22	0.12	IN
0.44	1.47	IN
0.77	0.55	IN
0.33	0.47	IN
0.99	0.18	IN
1.10	0.18	IN
0.99	1.65	IN
0.44	0.55	IN
0.55	0.13	IN
0.44	0.37	IN
0.44	0.55	IN
0.66	0.05	IN
0.55	0.29	IN
0.55	0.31	IN
1.43	0.23	IN
0.55	0.61	IN
0.33	0.33	IN
0.33	0.47	IN
0.55	0.92	IN
0.66	1.32	IN
0.88	0.49	IN
0.33	0.06	IN
0.66	0.41	IN
0.77	0.55	IN
0.66	0.60	IN
0.55	0.55	IN
0.77	0.37	IN
0.33	0.17	IN
0.22	0.28	IN
0.44	0.18	IN
1.65	0.72	IN
0.66	0.83	IN
0.55	0.46	IN
0.88	0.63	IN
0.55	0.46	IN
0.66	0.35	IN
2.20	0.05	IN

Real distance (µm)	Velocity (µm/s)	Directionality
5.06	1.27	IN
7.37	0.90	IN
0.99	0.16	IN
1.32	0.78	IN
0.22	0.05	IN
0.88	0.80	IN
0.55	0.31	IN
0.33	0.14	IN
0.55	0.55	IN
0.55	0.04	IN
0.55	0.69	IN
0.44	0.44	IN
1.32	0.25	IN
1.10	0.26	IN
0.88	0.44	IN
0.66	0.66	IN
-0.11	1.10	IN
-0.11	1.10	IN
-0.11	1.10	IN
-0.11	1.10	IN
-0.11	1.10	IN
0.44	0.63	OUT
0.44	0.49	OUT
1.43	1.43	OUT
1.21	0.93	OUT
0.55	0.79	OUT
0.44	0.63	OUT
0.44	1.47	OUT
1.10	0.65	OUT
1.54	0.18	OUT
0.44	0.63	OUT
0.55	0.42	OUT
0.88	0.68	OUT
0.88	0.59	OUT
0.44	0.63	OUT
0.33	0.41	OUT
0.33	0.21	OUT
0.33	0.41	OUT
0.55	0.37	OUT

Real distance (µm)	Velocity (µm/s)	Directionality
1.21	0.30	OUT
0.11	0.05	OUT
0.55	0.79	OUT
1.43	0.39	OUT
4.29	0.62	OUT
6.71	0.92	OUT
0.22	0.44	OUT
0.77	0.86	OUT
1.32	0.83	OUT
0.44	0.88	OUT
0.44	0.10	OUT
0.22	0.44	OUT
0.33	0.41	OUT
1.10	0.24	OUT
0.66	1.10	OUT
0.88	0.17	OUT
2.09	0.45	OUT
0.99	0.52	OUT
0.55	0.79	OUT
2.20	0.67	OUT
0.99	0.24	OUT
0.66	0.51	OUT
0.22	0.16	OUT
0.22	0.55	OUT
0.44	0.73	OUT
0.55	0.34	OUT
0.22	0.28	OUT
0.55	0.92	OUT
0.33	0.11	OUT
0.44	0.88	OUT
0.66	0.41	OUT
0.66	0.44	OUT
0.33	0.66	OUT
0.44	0.49	OUT
0.55	0.18	OUT
0.66	0.41	OUT
0.55	0.29	OUT
0.77	0.59	OUT
0.66	0.55	OUT

Real distance (µm)	Velocity (µm/s)	Directionality
0.77	0.70	OUT
0.77	0.45	OUT
0.66	0.11	OUT
1.10	0.05	OUT
0.44	0.40	OUT
0.44	0.23	OUT
0.44	0.13	OUT
0.44	0.23	OUT
0.33	0.47	OUT
0.55	0.79	OUT
0.33	0.55	OUT
0.88	0.88	OUT
0.22	0.24	OUT
0.44	0.34	OUT
0.33	0.17	OUT
0.55	0.05	OUT
0.33	0.37	OUT
0.99	0.13	OUT
0.44	0.21	OUT
0.33	0.66	OUT
0.44	0.49	OUT
0.22	0.37	OUT
0.33	0.21	OUT
0.99	0.66	OUT
0.33	0.17	OUT
0.22	0.18	OUT
0.66	0.47	OUT
0.22	0.37	OUT
0.33	1.10	OUT
0.66	0.66	OUT
0.44	0.23	OUT
0.55	0.18	OUT
0.44	0.16	OUT
0.55	0.21	OUT
0.44	0.37	OUT
0.55	0.31	OUT
0.33	0.25	OUT
0.66	0.51	OUT
0.33	0.33	OUT

Real distance (µm)	Velocity (µm/s)	Directionality
1.10	0.58	OUT
0.99	0.15	OUT
0.66	0.16	OUT
0.55	0.92	OUT
0.55	0.13	OUT

Real distance (µm)	Velocity (µm/s)	Directionality
0.55	0.69	OUT
0.44	0.28	OUT
0.88	0.68	OUT
0.22	0.44	OUT
1.43	0.43	OUT

HR

Real distance (µm)	Velocity (µm/s)	Directionality
0.44	0.10	IN
0.55	0.28	IN
2.75	0.47	IN
0.66	0.16	IN
0.55	0.69	IN
2.20	0.59	IN
0.55	0.69	IN
1.10	0.65	IN
0.66	1.32	IN
0.44	0.73	IN
1.10	0.19	IN
1.21	0.22	IN
0.55	0.39	IN
0.88	0.55	IN
0.77	0.77	IN
0.44	0.18	IN
0.55	0.42	IN
0.88	0.88	IN
0.55	1.10	IN
0.55	0.25	IN
0.44	0.73	IN
0.77	0.77	IN
1.43	0.35	IN
0.33	0.11	IN
0.22	0.20	IN
0.99	0.76	IN
1.43	0.46	IN
1.21	1.21	IN
1.21	0.48	IN
0.44	0.15	IN
2.86	0.89	IN

Real distance (µm)	Velocity (µm/s)	Directionality
0.44	0.34	IN
0.55	0.69	IN
0.55	0.09	IN
1.98	0.52	IN
0.33	0.16	IN
0.44	0.73	IN
0.66	0.55	IN
1.10	0.79	IN
0.55	0.10	IN
3.30	0.62	IN
0.44	0.49	IN
0.66	0.31	IN
0.55	0.32	IN
1.32	0.17	IN
0.88	0.13	IN
0.66	0.60	IN
1.21	0.30	IN
1.43	0.65	IN
0.66	0.83	IN
0.77	0.55	IN
0.99	0.58	IN
0.55	0.42	IN
1.87	1.25	IN
0.33	0.06	IN
0.66	0.21	IN
0.22	0.24	IN
0.33	0.33	IN
0.33	0.13	IN
0.66	0.33	IN
0.66	0.08	IN
0.66	0.44	IN

Real distance (µm)	Velocity (µm/s)	Directionality
0.66	0.44	IN
0.44	0.88	IN
0.11	0.37	IN
0.22	0.31	IN
0.44	0.73	IN
1.10	0.26	IN
0.33	0.47	IN
0.44	0.29	IN
1.65	1.18	IN
0.22	0.31	IN
0.99	0.99	IN
0.55	0.20	IN
0.22	0.44	IN
0.33	0.33	IN
0.33	0.16	IN
0.44	1.10	IN
1.32	0.24	IN
0.22	0.07	IN
1.10	0.69	IN
1.76	0.68	IN
0.44	0.28	IN
2.31	0.68	IN
0.55	0.14	IN
0.44	0.55	IN
0.66	0.60	IN
0.22	0.37	IN
0.77	0.59	IN
0.55	0.79	IN
0.44	0.31	IN
0.44	0.55	IN
0.55	0.14	IN
0.11	0.18	IN
0.44	0.55	IN
0.44	0.73	IN
0.44	0.73	IN
0.22	0.31	IN
0.33	0.47	IN
0.88	0.15	IN
0.33	0.41	IN

Real distance (µm)	Velocity (µm/s)	Directionality
1.32	0.16	IN
0.77	0.21	IN
0.33	0.22	IN
0.55	0.25	IN
0.66	0.35	IN
0.22	0.12	IN
0.55	0.61	IN
0.22	0.31	IN
2.53	0.51	IN
4.73	1.10	IN
4.18	0.80	IN
0.99	0.62	IN
0.44	0.22	IN
0.33	0.17	IN
0.55	0.14	IN
0.33	0.07	IN
0.55	0.24	IN
2.31	0.83	IN
0.33	0.55	IN
0.22	0.24	IN
0.11	0.16	IN
0.66	0.08	IN
0.33	0.17	IN
0.44	0.07	IN
0.55	0.06	IN
0.33	0.05	IN
0.44	0.06	IN
1.32	0.31	IN
0.77	0.48	IN
2.09	2.09	IN
0.77	0.64	IN
0.33	0.33	IN
0.33	0.37	IN
0.88	0.18	IN
1.87	0.29	IN
0.88	0.19	IN
3.08	0.36	IN
0.88	0.52	IN
0.44	0.06	IN

Real distance (µm)	Velocity (µm/s)	Directionality
0.66	0.23	IN
0.66	0.41	IN
0.22	0.10	IN
0.33	0.25	IN
0.66	0.44	IN
1.10	0.73	IN
0.77	0.70	IN
0.99	0.09	IN
0.33	0.22	IN
0.77	0.10	IN
1.21	0.53	IN
0.88	0.18	IN
0.33	0.16	IN
0.99	0.22	IN
0.22	0.37	IN
0.55	0.92	IN
0.33	0.66	IN
0.66	0.16	IN
0.66	0.55	IN
0.44	0.55	IN
0.55	0.42	IN
0.55	0.21	IN
0.55	0.69	IN
2.97	0.50	IN
0.22	0.15	IN
0.66	0.39	IN
0.55	0.42	IN
0.77	0.64	IN
0.44	0.23	IN
1.10	0.39	IN
1.43	0.18	IN
0.88	0.88	IN
0.55	0.61	IN
0.33	0.04	IN
0.33	0.08	IN
1.98	1.52	IN
4.73	1.13	IN
0.77	0.55	IN
0.55	0.39	IN

Real distance (µm)	Velocity (µm/s)	Directionality
1.54	0.08	IN
0.44	0.18	IN
0.77	0.35	IN
-0.11	1.10	IN
-0.11	1.10	IN
-0.11	1.10	IN
-0.11	1.10	IN
0.99	0.22	OUT
1.32	0.21	OUT
0.33	0.24	OUT
0.55	0.11	OUT
0.33	0.37	OUT
1.32	0.21	OUT
1.54	0.21	OUT
0.99	0.50	OUT
0.77	0.48	OUT
0.44	0.63	OUT
0.44	0.49	OUT
0.44	0.44	OUT
0.33	0.24	OUT
0.88	0.46	OUT
0.33	0.66	OUT
0.88	0.73	OUT
0.44	0.16	OUT
0.44	0.49	OUT
1.21	0.61	OUT
1.32	0.78	OUT
1.54	0.16	OUT
0.33	0.66	OUT
0.88	0.40	OUT
0.66	0.47	OUT
0.66	0.18	OUT
0.22	0.16	OUT
2.42	0.93	OUT
0.44	0.44	OUT
0.55	0.25	OUT
0.88	0.10	OUT
0.33	0.55	OUT
0.44	0.88	OUT

Real distance (µm)	Velocity (µm/s)	Directionality
0.66	0.73	OUT
5.72	0.91	OUT
0.11	0.28	OUT
0.77	0.10	OUT
0.22	0.22	OUT
0.44	0.49	OUT
1.10	0.50	OUT
0.77	0.15	OUT
0.66	1.10	OUT
0.99	0.58	OUT
0.33	1.10	OUT
0.33	0.37	OUT
0.22	0.55	OUT
0.33	0.37	OUT
0.22	0.24	OUT
0.55	0.37	OUT
0.99	0.62	OUT
1.87	2.34	OUT
0.44	0.55	OUT
1.32	0.83	OUT
0.66	0.73	OUT
0.77	1.10	OUT
0.44	0.49	OUT
0.44	0.20	OUT
0.44	1.47	OUT
0.33	0.11	OUT
1.65	0.18	OUT
1.10	0.48	OUT
0.66	0.17	OUT
0.55	0.50	OUT
2.09	0.91	OUT
0.44	0.88	OUT
0.66	0.18	OUT
0.22	2.20	OUT
1.32	1.32	OUT
0.99	1.24	OUT
1.10	0.10	OUT
0.44	0.55	OUT
0.44	0.55	OUT

Real distance (µm)	Velocity (µm/s)	Directionality
0.22	0.44	OUT
0.33	0.47	OUT
0.33	0.30	OUT
0.22	0.28	OUT
1.10	0.55	OUT
1.10	0.52	OUT
1.10	1.22	OUT
0.77	0.96	OUT
0.88	0.15	OUT
1.98	0.55	OUT
1.21	0.18	OUT
0.44	0.44	OUT
0.33	0.24	OUT
0.88	0.88	OUT
2.64	0.18	OUT
0.44	0.55	OUT
1.87	0.45	OUT
4.73	1.35	OUT
2.09	1.00	OUT
10.67	1.40	OUT
2.64	1.32	OUT
0.88	0.18	OUT
0.33	0.13	OUT
0.33	0.66	OUT
2.53	0.94	OUT
4.18	0.37	OUT
2.53	0.87	OUT
0.22	0.31	OUT
0.33	0.25	OUT
0.22	0.37	OUT
1.32	0.11	OUT
1.65	0.15	OUT
0.55	0.61	OUT
0.55	0.46	OUT
0.55	0.26	OUT
0.44	0.44	OUT
0.77	0.45	OUT
1.54	0.62	OUT
0.66	0.55	OUT

Real distance (µm)	Velocity (µm/s)	Directionality
0.99	0.08	OUT
0.44	0.73	OUT
0.55	0.12	OUT
1.98	0.66	OUT
0.77	0.23	OUT
1.10	1.10	OUT
0.88	0.88	OUT
0.33	0.55	OUT
1.98	0.43	OUT
0.44	0.55	OUT
0.33	0.33	OUT
0.33	0.47	OUT
0.99	0.09	OUT
0.55	0.31	OUT
0.22	0.55	OUT

0.55	0.79	OUT
Real distance (µm)	**Velocity (µm/s)**	**Directionality**
1.10	0.50	OUT
1.43	0.27	OUT
0.88	1.76	OUT
0.33	0.11	OUT
0.44	0.14	OUT
0.77	0.77	OUT
0.55	0.61	OUT
0.55	0.69	OUT
0.33	0.13	OUT
0.99	0.66	OUT
5.06	0.77	OUT
1.65	1.03	OUT
0.33	0.16	OUT
0.77	0.51	OUT

RR

Real distance (µm)	Velocity (µm/s)	Directionality
0.55	0.34	IN
0.77	0.51	IN
0.33	0.09	IN
0.22	0.14	IN
0.77	0.64	IN
3.41	0.85	IN
1.32	1.20	IN
1.32	0.88	IN
1.21	0.55	IN
3.85	0.19	IN
1.76	0.09	IN
2.20	0.59	IN
0.33	0.12	IN
0.77	0.43	IN
0.88	0.07	IN
1.21	0.81	IN
0.22	0.17	IN
0.66	0.83	IN
0.66	0.19	IN

Real distance (µm)	Velocity (µm/s)	Directionality
0.66	0.12	IN
0.44	0.88	IN
0.77	0.14	IN
0.66	0.94	IN
0.44	0.49	IN
0.22	0.22	IN
0.88	0.52	IN
1.87	0.85	IN
1.32	0.38	IN
0.55	0.31	IN
0.44	0.63	IN
0.33	0.17	IN
0.44	0.08	IN
0.33	0.33	IN
0.22	0.16	IN
0.55	1.10	IN
0.99	0.15	IN
0.44	0.10	IN
2.42	0.47	IN

Real distance (µm)	Velocity (µm/s)	Directionality
1.87	0.16	IN
0.44	0.49	IN
2.86	0.65	IN
0.88	0.38	IN
0.44	0.11	IN
1.10	0.18	IN
0.66	0.10	IN
1.65	0.06	IN
0.44	0.88	IN
0.33	0.66	IN
0.22	0.10	IN
0.55	0.23	IN
0.66	0.33	IN
0.44	0.37	IN
1.10	0.52	IN
0.44	0.10	IN
0.88	0.55	IN
0.99	0.26	IN
0.88	0.13	IN
1.76	0.93	IN
0.77	0.20	IN
0.44	0.44	IN
0.22	0.28	IN
0.77	0.15	IN
0.22	0.55	IN
0.55	0.55	IN
1.65	0.25	IN
0.33	0.37	IN
0.77	0.51	IN
1.87	0.23	IN
1.10	0.14	IN
0.88	0.68	IN
1.10	0.92	IN
5.17	0.62	IN
1.65	0.10	IN
0.33	0.09	IN
0.66	0.60	IN
0.33	0.30	IN
1.10	0.73	IN

Real distance (µm)	Velocity (µm/s)	Directionality
0.33	0.30	IN
0.77	0.37	IN
0.77	0.77	IN
0.22	0.73	IN
0.33	0.09	IN
0.99	0.08	IN
2.75	0.25	IN
2.31	0.77	IN
0.44	0.14	IN
0.44	0.08	IN
0.33	0.47	IN
0.22	0.73	IN
0.66	0.66	IN
0.22	0.44	IN
0.22	0.03	IN
0.11	0.03	IN
1.32	1.47	IN
0.44	0.05	IN
0.33	0.41	IN
3.41	1.55	IN
1.54	1.10	IN
0.55	0.50	IN
0.44	0.31	IN
1.65	1.18	IN
1.32	1.10	IN
2.42	0.46	IN
0.22	0.22	IN
0.44	0.05	IN
0.55	0.69	IN
0.55	0.92	IN
0.44	0.18	IN
0.33	0.11	IN
0.33	0.55	IN
0.33	0.37	OUT
0.44	0.12	OUT
0.55	0.55	OUT
0.55	0.50	OUT
0.33	0.66	OUT
0.88	0.52	OUT

Real distance (µm)	Velocity (µm/s)	Directionality
0.77	0.86	OUT
2.09	0.75	OUT
0.77	0.96	OUT
0.88	0.55	OUT
0.55	0.18	OUT
0.33	0.33	OUT
0.55	0.69	OUT
0.55	1.38	OUT
0.44	0.88	OUT
0.55	0.37	OUT
0.22	0.10	OUT
0.88	0.18	OUT
0.33	0.14	OUT
1.32	0.44	OUT
0.66	0.23	OUT
1.10	0.27	OUT
1.10	0.73	OUT
2.31	0.49	OUT
0.77	0.16	OUT
0.33	0.47	OUT
0.88	0.04	OUT
0.55	0.79	OUT
0.99	0.14	OUT
0.33	0.47	OUT
0.55	1.10	OUT
0.44	0.24	OUT
0.55	0.31	OUT
0.55	0.14	OUT
0.44	0.22	OUT
1.10	0.69	OUT
0.99	0.50	OUT
1.65	0.47	OUT
1.54	0.64	OUT
0.33	0.22	OUT
1.43	0.37	OUT
0.88	0.59	OUT
0.44	0.12	OUT
0.33	0.19	OUT
0.33	0.33	OUT

Real distance (µm)	Velocity (µm/s)	Directionality
0.55	0.34	OUT
2.31	0.51	OUT
0.55	0.55	OUT
0.88	0.29	OUT
1.76	0.84	OUT
1.10	0.48	OUT
0.22	0.22	OUT
0.33	0.21	OUT
0.33	0.55	OUT
0.77	0.31	OUT
1.43	0.55	OUT
0.88	0.42	OUT
0.99	0.11	OUT
0.44	0.63	OUT
0.44	0.55	OUT
0.88	0.08	OUT
0.88	0.80	OUT
1.21	0.18	OUT
2.09	0.39	OUT
2.09	0.11	OUT
3.63	1.13	OUT
0.33	0.33	OUT
2.31	0.72	OUT
0.66	0.55	OUT
0.66	0.09	OUT
0.88	0.21	OUT
0.66	0.05	OUT
0.33	0.47	OUT
0.22	0.55	OUT
1.10	0.09	OUT
0.11	0.22	OUT
0.33	0.14	OUT
0.66	0.73	OUT
0.77	0.45	OUT
0.33	0.03	OUT
1.32	0.88	OUT
0.33	0.47	OUT
0.77	0.96	OUT
0.66	0.20	OUT

Real distance (µm)	**Velocity (µm/s)**	**Directionality**
0.33	0.55	OUT
0.55	1.10	OUT
0.22	0.10	OUT
0.22	0.55	OUT
0.88	1.10	OUT
0.33	0.37	OUT
0.22	0.31	OUT
0.55	0.55	OUT